

Dropping Geocontainers in Water

Absenken von Geocontainern im Wasser

Dr.-Ing. Fursan Hamad; Prof. Dr.-Ing. habil. Christian Moormann,
Universität Stuttgart, Institut für Geotechnik

In coastal engineering, geocontainers are becoming more frequently used instead of conventional materials. Dropping geocontainers in water has many applications varying from constructing dams to disposing materials. Different numerical models can be adopted according to the problem type though there is no unified scheme to include all complexities of the problem. The Material Point Method (MPM) is a numerical framework represents the continuum field as Lagrangian material points (particles), which can move through a fixed background computational mesh. Thin-membrane and geotextile are integrated by modifying the algorithm to cope with the plane-stress condition of the thin-structure. Interaction of soil-geotextile is treated inherently in MPM using no-slip condition. Owing to the fact that the method accommodated material convection by the movement of the particles, fluids are treated similarly to solids in MPM considering the corresponding difference in the material law.

In this paper, the dynamics of dropping geocontainers in water is simulated. In order to mitigate the problem of mesh locking corresponding to the use of high bulk modulus for fluid, double enhancement techniques have been applied. The releasing of a geocontainer from a split barge is performed dry, where frictional contact between the geotextile and the barge is considered. The effect of geocontainer interaction has been investigated by dropping a second container. Next, the field test of dropping 130 m³ geocontainer is reproduced where more focus has been paid to the evolution of the geotextile forces. The problem is approximated as a two-dimensional although the present implementation is three-dimensional. At the end of the analysis, the dropping velocity as well as the pressure inside the soil are traced and compared to the available field measurements.

Im Wasserbau im Küstenbereich werden Geocontainer zunehmend anstelle von konventionellen Materialien eingesetzt. Das Absenken von Geocontainern im Wasser hat viele Einsatzbereiche, die vom Dammbau bis zur Entsorgung von Materialien reichen. Je nach Art des Problems können verschiedene numerische Modelle angewendet werden. Es gibt jedoch kein einheitliches Schema, welches alle Komplexitäten eines Problems abdecken könnte. Die Material-Point-Methode (MPM) ist ein numerischer Rahmen, mit dem das Kontinuumfeld in Form von Materialpunkten (Partikeln) nach Lagrange, die sich durch ein festes Berechnungsnetz im Hintergrund bewegen können, dargestellt wird. Dünne Membrane und Geotextilien werden durch Anpassung des Algorithmus integriert, um den ebenen Spannungszustand der dünnen Konstruktion zu berücksichtigen. Die Wechselwirkung zwischen dem Boden und dem Geotextil wird bei der Material-Point-Methode unter Anwendung der Haftbedingung behandelt. Da in der MPM-Methode die Konvektion von Material durch die Bewegung von Partikeln erfasst wird, werden in dieser Methode Flüssigkeiten auf die gleiche Weise wie Feststoffe unter Berücksichtigung der entsprechenden Unterschiede im Materialgesetz behandelt.

In diesem Beitrag wird die Dynamik beim Absenken von Geocontainern im Wasser simuliert. Um die Problematik eines Blockierens des Netzes, was der Anwendung eines hohen Kompressionsmoduls für Flüssigkeiten entspricht, zu verringern, wurde das Verfahren zweifach erweitert. Das Ablassen eines Geocontainers von einer Klappschute wird unter trockenen Bedingungen und unter Berücksichtigung des Reibungskontakts zwischen dem Geotextil und der Klappschute durchgeführt. Die Wirkung der Interaktion des Geocontainers wurde durch Absenken eines zweiten Geocontainers untersucht. Anschließend wird der Feldversuch, bei

dem ein Geocontainer mit einem Volumen von 130 m³ abgeseht wurde, reproduziert, wobei hier der Schwerpunkt eher auf die Entwicklung der auf das Geotextil ausgeübten Kräfte gelegt wird. Das Problem wird als zweidimensional genähert, auch wenn die gegenwärtige Umsetzung dreidimensional ist. Am Ende der Analyse werden sowohl die Absenkgeschwindigkeit als auch der Druck im Boden aufgezeichnet und mit den vorliegenden Feldmessungen verglichen.

1 Introduction

Einleitung

The applications of geosynthetic materials are increasing especially in the field of coastal and hydraulic engineering where the thin material is combined with dredged materials to provide an efficient alternative for conventional materials (Pilarczyk, 2000). *Geocontainers*, in which a prefabricated geotextile is placed in a split barge and mechanically filled with sand or slurry, were developed during the late eighties. The container is then dumped from the scow bed into the desired position. Single or multiple geocontainers can be placed for shore protection, including breakwaters. Geocontainers and in particular geotextiles can experience high stresses. Deltares carried out several field and lab tests to study the placement history of the containers, which included measuring the fall velocity and strains (Bezuijen et al. 2002a; 2002b). One of the major concerns associated with dropping geocontainers is the strength of the fabric and the seam. The geotextile should resist the forces during filling, releasing and impacting of the seabed. The risk of bursting geocontainers in deep water, inaccurate placement due to waves and current, or even slope failure of a heap of geocontainers are important issues for the feasibility of using geocontainers (Groot et al. 2004). Failure of geocontainers can be correlated to high forces in the geotextile when compared with its ultimate strength. Maximum forces are expected to occur during the releasing from the bin and the impacting on the ground, which is largely controlled by the amount of filling, the barge design, and the falling height.

The numerical modelling of the thin-walled structures joined with history-dependent material subjected to large deformation in the presence of water is a challenging topic for traditional methods. Simulation of the

entire process contributes to the understanding of the flow field around the container, particularly when a geocontainer hits the ground. In order to avoid problems associated with mesh distortion and element entanglement in the Lagrangian finite element methods, large deformation problem can be solved using *meshfree methods*. These methods trace the history of the state variables at material points that are independent of the mesh. Since the mesh does not deform, the problem of severe mesh distortion is overcome. An example of these methods is the Smoothed Particle Hydrodynamics (SPH), which is widely used in fluid and solid dynamics (cf. Lucy, 1977). One such method is the particle-in-cell method (PIC), which was used to model fluid dynamics in the 1960s. The PIC method was adopted by Sulsky et al. (1995) for solid mechanics, later giving it the name material point method (MPM). MPM represents the continuum by a collection of material points (particles), whereas information is transferred from these points to the background computational grid. Because of the arbitrary Lagrangian-Eulerian description of material, the method is best suited for large deformation in fluid and solid mechanics. The computational framework in MPM allows including various materials as well as structural elements, considering the difference in the material evolution. The method has been successfully applied to various geotechnical problems including discharge of granular material from a silo (Wieckowski et al., 1999), dropping geocontainers from a split barge (Hamad et al., 2012), and more (Jassim et al., 2011; York et al., 1999).

In this paper, the MPM is introduced as a unified computational framework to handle the interaction of soil, water and geotextile in dropping geocontainers. To alleviate the locking problem associated with using the low-order element in MPM for nearly incompressible fluid, enhanced algorithm has been tested for a practical application of the geotube, for which the analytical solution for simplified model is available. The aim of the comparison is to evaluate the MPM fluid modelling as it converges to the steady-state solution and the interaction with the geotextile elements. The releasing of the soil containers is performed dry where folds, which are provided in practice, are simplified by adding slack along the geotextile. In order to study the interaction effect of more geocontainers, an installed container on a soil bed is followed by second one where interaction between the two is taking place. Dropping a geocontainer in water reduces the dumping velocity because of the

drag forces. In order to predict the container terminal velocity properly, the numerical model should be able to reproduce the fluid velocity field and the interaction with the sinking body. The last part of this paper is to simulate the dropping of geocontainer in water and to compare the results with the available measurement data.

2 A unified framework of MPM *Einheitlicher Rahmen der MPM*

In MPM, the computational domain is discretised using two type of discretisations. The first is the Lagrangian discretisation where the continuum body is represented by material points, or particles, which are tracked during the computation. To solve the momentum equation, the computational mesh is introduced as a second discretisation that provides a convenient means of calculating discrete derivatives and carrying out integration. Whereas for FEM, the material points are tied tightly to the elements, for MPM the material points are allowed to move from one element to another in Eulerian fashion such that the state properties remain with the material points. Care should be taken here to make a clear distinction between pure Eulerian process, where the total derivative of local and convective components is applied, while the latter does not exist within the MPM framework. Giving that the movement of the Lagrangian material points through the computational cell is traced, the convection of the material is resembled naturally. Illustration of MPM discretisations for a continuum body is shown in Figure 1.

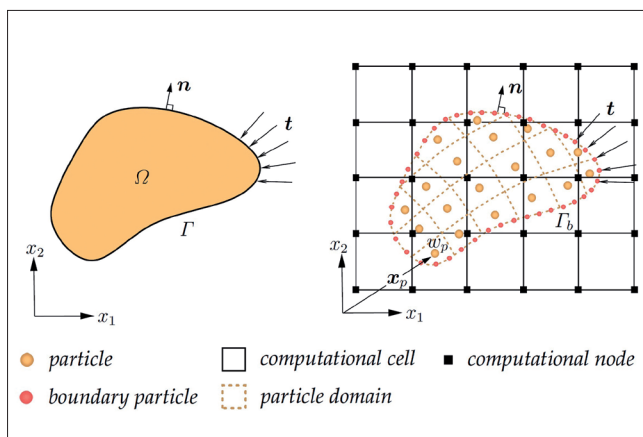


Figure 1: Continuum body (left) discretised with MPM (right)
Bild 1: Kontinuum (links), Diskretisierung mit MPM (rechts)

2.1 Spatial and time discretisations

Räumliche und zeitliche Diskretisierungen

In this paper, we follow the original MPM formulation (Sulsky et al., 1995), in which a body is defined in terms of material points. In other words, the properties and state variables such as stress and momentum are collocated at the material points. As shown in Figure 1, the continuum body Ω is discretised into subdomains, where the mass of the subdomain w is concentrated at the location \mathbf{x}_p of the material point p such that

$$\rho(\mathbf{x}) = \sum_{p=1}^{n_p} m_p \delta'(\mathbf{x} - \mathbf{x}_p) \quad (1)$$

in which ρ being the material density, m_p is the mass of the material point p , n_p is the number of material points, and the Dirac delta function δ' is defined by

$$\delta'(\mathbf{x} - \mathbf{x}_p) = \begin{cases} 0, & \mathbf{x} \neq \mathbf{x}_p \\ +\infty, & \mathbf{x} = \mathbf{x}_p \end{cases}$$

with

$$\int_{-\infty}^{+\infty} \delta'(\mathbf{x} - \mathbf{x}_p) d\mathbf{x} = 1 \quad (2)$$

where Equation (1) is not applicable to the boundary particles, see Figure 1, as these particles represent the boundary Γ . The concept of performing integration at material concentration point in MPM is similar to FEM, except that the material points are able to move within the computation and therefore not to be surely at the Gaussian point. We start with the conservation of linear momentum

$$\rho \ddot{\mathbf{u}} = \nabla \cdot \boldsymbol{\sigma} + \rho \mathbf{g} \quad \text{and} \quad \mathbf{t} = \boldsymbol{\sigma} \cdot \mathbf{n} \quad (3)$$

with \mathbf{u} is the displacement, a superposed dot denotes differentiation with time, $\boldsymbol{\sigma}$ denotes the Cauchy stress tensor and \mathbf{g} is the gravitational acceleration vector. The surface traction acting on the external boundary is denoted by \mathbf{t} and \mathbf{n} is the outward unit normal of the boundary. Applying the virtual work principle on a domain of volume V surrounded by boundary S yields

$$\int_V \delta \mathbf{u}^T \rho \ddot{\mathbf{u}} dV = - \int_V \delta \boldsymbol{\varepsilon}^T \boldsymbol{\sigma} dV + \int_V \delta \mathbf{u}^T \rho \mathbf{g} dV + \int_S \delta \mathbf{u}^T \mathbf{t} dS \quad (4)$$

where δ implies a virtual quantity, $\boldsymbol{\varepsilon}$ is the strain tensor and the script T denotes the transpose.

For space discretisation, the displacement field \mathbf{u} is approximated in terms of interpolation functions \mathbf{N} and nodal displacements \mathbf{a} by $\mathbf{u} = \mathbf{N}\mathbf{a}$. The strain tensor is now written in vector notation as

$$\boldsymbol{\varepsilon} = \mathbf{B}\mathbf{a} \quad \text{with} \quad \mathbf{B} = \mathbf{L}\mathbf{N} \quad (5)$$

where \mathbf{B} is the usual finite element strain-displacement matrix, as computed from the linear differential operator \mathbf{L} and the shape functions \mathbf{N} . Substituting Equation (5) into Equation (4) gives

$$\delta \mathbf{a}^T \mathbf{M} \ddot{\mathbf{a}} = \delta \mathbf{a}^T (\mathbf{F}^{ext} - \mathbf{F}^{int}) \quad \text{or} \quad \mathbf{M} \ddot{\mathbf{a}} = \mathbf{F}^{ext} - \mathbf{F}^{int} \quad (6)$$

in which

$$\mathbf{M} = \int_V \rho \mathbf{N}^T \mathbf{N} dV, \quad \mathbf{F}^{ext} = \int_V \rho \mathbf{N}^T \mathbf{g} dV + \int_S \mathbf{N}^T \mathbf{t} dS$$

and $\mathbf{F}^{int} = \int_V \mathbf{B}^T \boldsymbol{\sigma} dV \quad (7)$

in which \mathbf{M} is the consistent mass matrix, \mathbf{F}^{int} and \mathbf{F}^{ext} are the internal and external forces, respectively. Equation (6) is identically used within FEM and MPM. However, in the Material Point Method \mathbf{M} can also change in size when particles move into empty elements. In other words, the total number of degrees-of-freedom of the system can vary. A lumped-mass matrix, which offers computational and storage advantages, is used instead of the consistent-mass matrix defined in Equation (7). The internal force in Equation (6) is represented by

$$\mathbf{F}^{int} = \int_V \mathbf{B}^T \boldsymbol{\sigma} dV \approx \sum_{p=1}^{n_p} \mathbf{B}_p^T \boldsymbol{\sigma}_p V_p \quad (8)$$

where n_p denotes the number of particles, and V_p is the volume associated with particle p .

The momentum equation is solved on the background computational mesh, which provides a convenient means for calculating discrete derivatives and carrying out integration. As illustrated in Figure 2, the MPM calculation cycle goes through three phases: Initialisation where information is transferred from material points to the computational grid nodes; Lagrangian phase that parallels a finite element calculation where the system

equations are setup and primary variables (velocity and displacement) are evaluated at the nodes, with stresses and strains determined at material points; and a convection phase where the location of particles and state variables are updated.

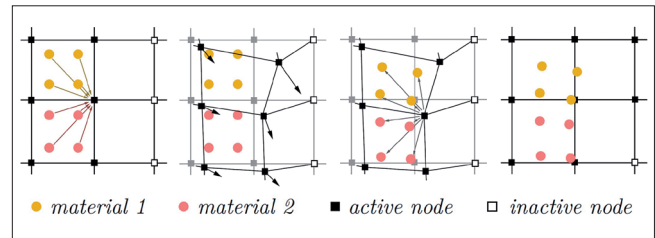


Figure 2: Solution procedure of the MPM computational step

Bild 2: Verfahren zur Lösung des Berechnungsschrittes in der MPM

On applying Euler-forward time integration with lumped-mass matrix, Equation (6) yields

$$\dot{\mathbf{a}}^{t+\Delta t} = \dot{\mathbf{a}}^t + \Delta t \ddot{\mathbf{a}}^t, \quad \ddot{\mathbf{a}}^t = [\mathbf{M}_L^t]^{-1} \mathbf{F}^t \quad (9)$$

where Δt is the current time increment, $\mathbf{F} = \mathbf{F}^{ext} - \mathbf{F}^{int}$, $\dot{\mathbf{a}}^t$ and $\dot{\mathbf{a}}^{t+\Delta t}$ are the nodal velocities at time t and $t+\Delta t$, respectively. The incremental nodal displacement is obtained by integrating the nodal velocity by the Euler-backward rule and the position of the particles are subsequently updated, i.e.

$$\Delta \mathbf{a}^{t+\Delta t} = \Delta t \dot{\mathbf{a}}^{t+\Delta t}, \quad \mathbf{x}_p^{t+\Delta t} = \mathbf{x}_p^t + \mathbf{N}_p \Delta \mathbf{a}^{t+\Delta t} \quad (10)$$

where \mathbf{x}_p^t and $\mathbf{x}_p^{t+\Delta t}$ are the particle positions at time t

and $t+\Delta t$, respectively. Strains and stresses at particles are updated using the same algorithms as for Gaussian integration points within the standard FEM. In updated Lagrangian FEM, one would use $\Delta \mathbf{a}$ to update the finite element mesh, but within the MPM only particles positions are updated. Particles eventually cross element boundaries, which entails that the new element of a crossing particle has to be detected.

3 Geotextile tube (geotube) Geotextilschlauch (Geotube)

The geotextile tube, or *geotube*, is a tube formed in-situ consisting of permeable but soil-tight geotextile (Pilarczyk, 2000). Geotubes are widely used for appli-

cations in coastal and hydraulic engineering where the gravity barrier type structures are required. In practice, a computer program based on equilibrium equations is commonly used to find the pressure distribution and the final configuration according to the amount of pumped liquid (Leshchinsky et al., 1996).

In order to examine the applicability of combining the enhancement schemes for the liquid-behaviour materials in MPM (Stolle et al., 2014), the geotube problem is simulated numerically and compared to the closed-form solution. Moreover about the aim of this comparison is to validate the geotextile-water interaction model and the efficiency of the MPM algorithm to converge toward the steady-state solution. The thin-structure is treated as a finite element structure in the MPM framework using the Couple FEM-MPM approach (Hamad et al., 2014). On the other hand, enhancement techniques are applied for the nearly-incompressible fluid to mitigate the mesh locking problem associated with the high bulk modulus. Dynamic relaxation scheme is employed where two convergence criteria are introduced to ensure the minor effect of dynamics. Although the analysis is performed for two-dimensional problem, however, the formulation is three-dimensional using four-node tetrahedral elements.

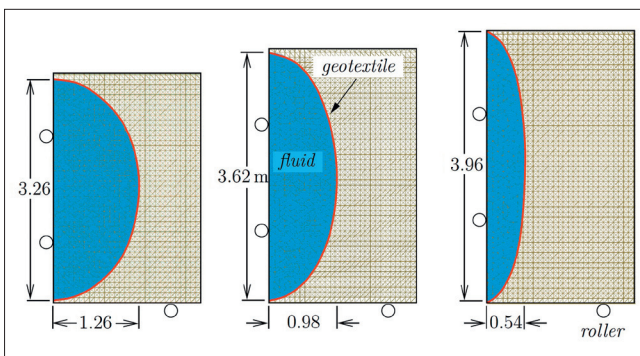


Figure 3: Initial configuration of the MPM model for different geotubes filling

Bild 3: Anfängliche Konfiguration des MPM-Modells für verschiedene Geotube-Füllungen

For the sake of comparison, three different filling ratios for the geotube are modelled, where zero stress state is initially assigned to all material points with gravity being the only external force. The initial shapes of the numerical model are assumed as ellipses as depicted in Figure 3, which are seated on a smooth ground to arrive eventually to the final quasi-static shape. The unit weight of the filling fluid is $\gamma_f = 12 \text{ kN/m}^3$ and the

circumference length of the geotextile is 9.2 m. Filling inside the tubes is indicated in terms of cross-sectional area 6.45, 5.56 and 3.36 m^2 , which give a corresponding final configuration $H/W = 0.78$, 0.50 and 0.22 where H and W are the final height and width of the tube, respectively. The elastic thin-structure is given very high tensile strength to be assumed inextensible. The fluid is modelled with bulk modulus $K_f = 2.13 \text{ GPa}$ and relatively high viscosity $m = 1.0 \text{ Pa}\cdot\text{s}$, which works as an artificial damping to converge faster to the quasi-static solution.

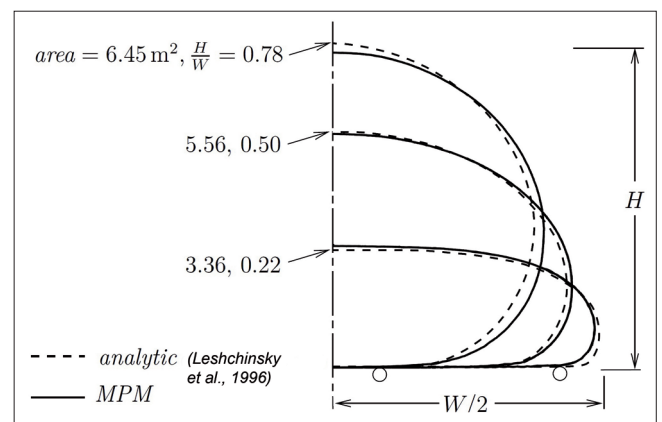


Figure 4: Final configuration of the geotextile tube

Bild 4: Endgültige Konfiguration des Geotextilschlauchs

After letting the initial, assumed profile of the geotextile tube rest on the smooth ground, it keeps bouncing up and down for few cycles. Two criteria had to be satisfied for checking the quasi-static solution: the overall kinetic energy, and the out-of-balance between external and internal forces must meet certain tolerance; e.g. a tolerance of 0.05 is selected for both criteria in the geotube application. At the quasi-static state, the MPM geotextile for the final shape of the tube is compared with the analytical solution as shown in Figure 4. Considering the approximation of the initial configuration, the MPM profiles are close except for some small deviation in the case of high and low filling.

Looking at the pressure distribution of the moderate filling in Figure 5, the MPM shows a good reproduction of the linear pressure variation. This is attributed to the applied enhancement technique. The fact that the locking mitigation does spatial averaging, the layering of the pressure distribution has some wrinkles. As a summary for the geotube problem, the MPM fluid model in combination with the geotextile is able to reproduce the quasi-static solution.

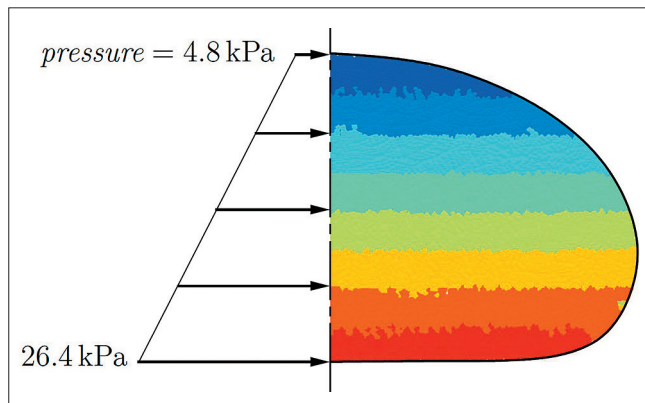


Figure 5: Pressure distribution in the tube with 5.56 m^2 filling: (left) analytical solution after Leshchinsky et al. (1996) and (right) MPM with the range 4.4 to 26.7 kPa

Bild 5: Druckverteilung im Schlauch mit einer Füllung mit einem Volumen von $5,56 \text{ m}^2$: (links) analytische Lösung nach Leshchinsky et al. (1996) und (rechts) MPM im Bereich 4,4 bis 26,7 kPa

4 Dropping dry geocontainers

Absenken von trockenen Geocontainern

Another application of geotextiles is for the construction of geocontainer units, which consist of a prefabricated geotextile placed in a split barge and mechanically filled with sand or slurry up to several hundred cubic meters. They are subsequently dumped from the scow bed in the desired position. Geocontainer units are used for underwater structures such as breakwaters, barriers to close openings, and dams that hold contaminated sludges. See, for example, Pilarczyk (2000) for other applications.

Due to the complexity of the problem, the understanding of what happens to a container during release and its interaction with other geocontainers is still poor. In this regard, theoretical models based on equilibrium have helped to identify the sensitivity of the forces that develop to physical variables (Groot et al., 2000). Furthermore, large scale physical model tests have provided data that can be used to realistically estimate the deformation and pressure developed inside the geocontainer; although it has been difficult to reproduce measured values due to variation of the control parameters from one test to another (Bezuijen et al., 2002a). For better understanding of the accurate placement of geocontainers, physical model and numerical tests were conducted on a scaled simplified geocon-

tainer. Nevertheless, there is a need to investigate each step of the process separately and establish the variations of stresses associated with the large deformations that take place in the big soil bags. This can be accomplished by using continuum models. Hamad et al. (2013) adopted the material point method to model the release phase of the geocontainer from the split barge, which was considered as a nearly quasi-static process. The example given here focuses on the dropping of geocontainer on foundation soil followed by dropping a second container to see the effect of geocontainer interaction.

4.1 Releasing geocontainers

Ablassen von Geocontainern

The first important loading of the geotextile is when the barge opens and the geotextile is stretched across the opening. Four stages are distinguished for the opening of the barge and releasing the geocontainer (Groot et al., 2000). The first stage begins by stretching and uplifting the lower part of the geocontainer. As the container descends without much deformation in the second stage, more deformation is taking place in the third stage while it is passing through the opening. Finally, the whole container goes through the opening although the open is kept constant. Numerous methods are presented in literature focusing on these stages, but mainly on the last one to predict the geotextile forces at the releasing moment. Most of these methods however are based on dividing the container into rigid blocks where the interaction forces are obtained from the mobilised friction at failure combined with equilibrium state; for more details see (Pilarczyk, 2000).

Depending on the particular parameter being measured in the dropping process, experimental model tests are performed differently. For instance dropping geocontainer in air can be used when the tensile forces and the soil deformation are more important than the flow resistance. Furthermore, the barge profile has an influence on the smooth unloading of the container. A sudden opening of the bin reduces the forces that develop. The focus of the MPM model is to model the salient features associated with installing geocontainers.

The analysed problem is similar to that discussed by Groot et al. (2000), in which a container having a per-

centage of fill of approximately 58% is dropped in place. The percentage of fill refers to the actual fill volume divided by the maximum possible fill volume that allows a container to comfortably pass through the barge bottom. In our case, the container is falling through air and not water, which implies that the effective unit weight and the velocity of the container before impact are higher than would be encountered in practice. Thus the stress predictions are expected to be higher than those developed when a container falls through water. Nevertheless, the example demonstrates the ability of the MPM to capture the physics associated with allowing a container to drop into place, as well as interact with a second container.

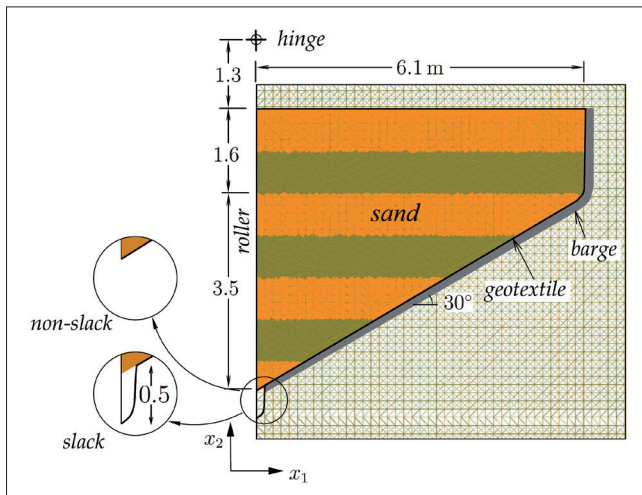


Figure 6: Initial MPM configuration of releasing geocontainer from a split barge

Bild 6: Anfängliche MPM-Konfiguration des Ablassens eines Geocontainers von einer Klappschute

Figure 6 depicts the problem and shows the MPM discretisation. A two-dimensional problem is analysed using a three-dimensional model. The initial location of the container is 8 m above the ground that consists of a 1.5 m layer of soil. The bottom boundary of the ground layer is assumed fully fixed; however, viscous boundary can be added there to reduce the effect of reflecting waves (Jassim et al., 2011). Much of the domain consists of empty elements. An element is not considered in the computation until it contains at least one particle. The placement process is simulated by allowing the barge to open with an angular velocity of 1 rad/s. The geotextile is modelled as a linear-elastic material having an axial stiffness of 400 kN/m and negligible density. An elastic-perfectly plastic Mohr-Coulomb model is adopted for the soil. Assuming the soil inside the container

is very loose, its elastic modulus is estimated to have a value 820 kPa whereas that of the ground is assumed to be 6000 kPa. The unit weight of the soil inside the container and that of the ground is taken as 18 and 20 kN/m³, respectively, with both soils having a friction angle 30°, zero dilatancy, 0.333 Poisson's ratio and cohesion of 1 kPa. A dynamic friction coefficient of 0.3 is adopted when modelling the resistance that develops between the geotextile of the container and the bottom of the barge. A similar value of friction coefficient is used for geotextile-geotextile and geotextile-ground soil contact.

Considering that the opening phase is achieved slowly, the process is nearly quasi-static, therefore, the force equilibrium shown in Figure 7 is applicable. In this figure, the force (F_s) representing the load that squeezes the soil results from the horizontal stress in soil integrated along the plane symmetry. Moreover, the normal reaction force to the barge (F_n) produces the frictional force (μF_n). All these forces plus gravity and the geotextile tensile force (F_{GT}) should keep the geocontainer in place when the barge stops opening.

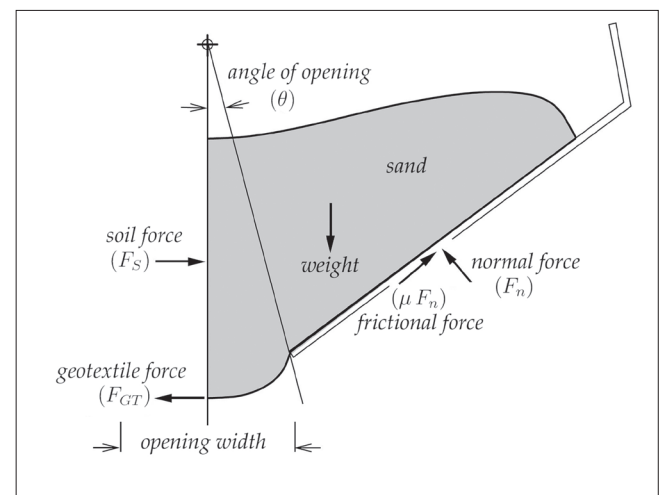


Figure 7: Equilibrium forces on the geocontainer

Bild 7: Kräftegleichgewicht am Geocontainer

The development of the soil and geotextile forces with the opening angle (θ) is shown in Figure 8. The small drop at the beginning of the soil force is most likely related to the assumption of the initial equilibrium with K_0 procedure, which quickly varies linearly. On the other hand, the geotextile force starts from a zero value, tending to also follow a straight line trend. The sharp drop in the soil force and the corresponding increase in the geotextile tension are indications that the soil becomes

more free to dilate outside the barge. After this point, the two forces (F_S) and (F_{GT}) eventually approach each other, which tells that the barge does not apply any significant force on the geocontainer (Hamad et al., 2012). As the barge opening increases, tensile forces in the geotextile (F_{GT}) increase as they keep the soil together. Eventually, these forces pull the soil away from the barge, which in turn decreases the frictional forces between the geotextile and the barge. As a result, the geocontainer loses contact gradually with increasing angle of opening. Holding quasi-static equilibrium, the difference between the soil and geotextile force increases with loading, which is due to the loss of contact during the releasing. Since the frictional force (μF_n) and the force normal to the barge (F_n) decrease, the term ($F_S - F_{GT}$) must increase to insure an equilibrium state. The linear variation between the two forces can be proven for the quasi-static equilibrium case (Pilarczyk, 2000).

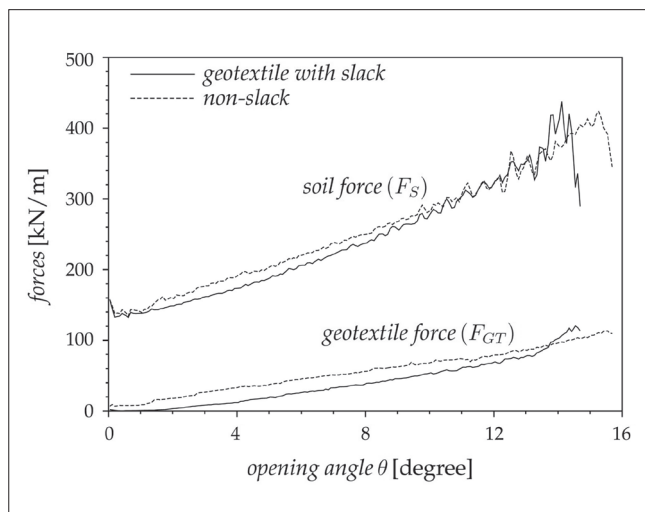


Figure 8: Development of forces in the geocontainer
Bild 8: Entwicklung von Kräften im Geocontainer

Comparing the forces for the geotextile (*with*) and (*without*) slack shows a small difference, which indicates that the one without slack experiences higher forces. The important gain of adding the extra slack is clearly demonstrated by having a releasing with opening angle of two degrees less as compared to that of the non-slack case, as shown in Figure 8.

Two snapshots of dropping a container are shown in Figure 9. The first shows the barge at maximum opening and the geocontainer is sliding out of the barge while its top part is squeezed toward the centerline. In the same figure, the deformed geocontainer shape af-

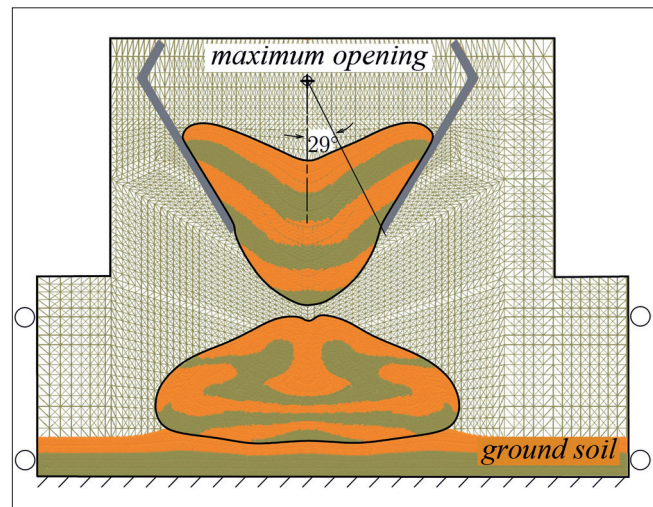


Figure 9: Snapshots for the first geocontainer during installation process

Bild 9: Momentaufnahmen des ersten Geocontainers während des Einbauvorgangs

ter hitting the ground is illustrated, which clearly shows by tracking the layering that the soil in the upper half is redistributing with the lower half compressing. In an actual application, where a container falls through water, this effect is expected to be less pronounced due to the effect of the water. After dropping the first geocontainer, the geocontainer seated on the ground such that it pushes the ground down and out under the container and up along the edges.

4.2 Interaction of geocontainers Wechselwirkung der Geocontainer

To construct an underwater structure, many containers are required. For example, the submerged containment dike on the river Elbe in Twielenfleth, Germany consists of more than 600 geocontainers, with each containing 300 m³ of soil (Tencate, 2007). As a first step of modelling such a structure, a second geocontainer is introduced in this study with 2 m offset to the right. At the end of the second bag installation, it is seen to have rotated on the first container and eventually rest partially on the ground as depicted in Figure 10. A large part of the second container is laying on the first one increasing its vertical stresses considerably. The fact that the ground layer is deformable has an impact on the uniformity of the stress distribution along the bottom of the first container. Again the small stress oscillation along the interface between the two geocontainers is related to the contact algorithm.

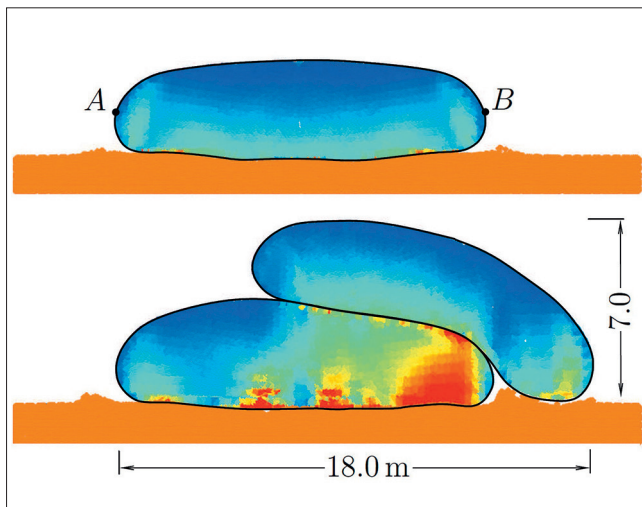


Figure 10: Vertical stress; blue colour is zero stress and red is -170 kN/m^2 : (top) after first geocontainer is released and (bottom) after the second is released

Bild 10: Vertikale Spannungen; wobei Blau keine Spannung und Rot -170 kN/m^2 bedeutet: (oben) nach Ablassen des ersten Geocontainers und (unten) nach Ablassen des zweiten Geocontainers

A last point to investigate in this study is the force variation developed along the geotextile upper surface A-B in Figure 10. The distribution of the tensile force per length of geocontainer (tensile stress in the geotextile times thickness) along the upper part of the first container is shown in Figure 11 after first stage of installation. The forces are in the range of 80-90 kN/m and almost equally distributed along the section. It goes up to 105 kN/m near to the centreline after the second installation stage. The figure shows that the forces at the far ends of the container are released especially where the second container is resting to the right as the soil inside is squeezed down. The maximum curve refers to the force variation in the membrane of the first geocontainer as it is being loaded by the second container at the time it reaches the most critical condition, which is about 7 sec before the final state. We see that there is an approximate 30 percent increase of the peak force relative to the peak force that develops after the second container has come to rest. In other words, the critical stress condition for design does not correspond to the final equilibrium state, but rather to time during impact before equilibrium is attained.

The simulation of dropping a geocontainer in place demonstrates that the MPM model is capable of predicting the shape and thickness of the container that is consistent with the criteria proposed by Pilarczyk (2000). The

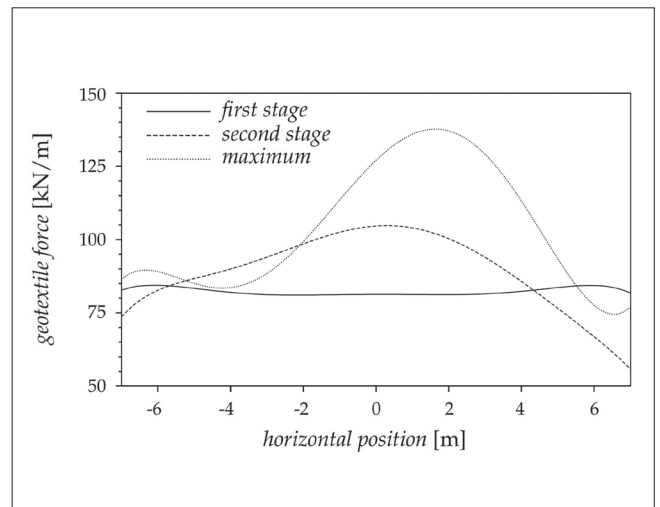


Figure 11: Geotextile forces along section A-B

Bild 11: Auf das Geotextil ausgeübte Kräfte entlang Schnitt A-B

model also predicts vertical stresses that are consistent with what one would expect. It is also shown that the formulation can handle the interaction of two containers.

5 Dumping of geocontainers in water *Verklappen von Geocontainern im Wasser*

Dumping geocontainers in water has many applications varying from constructing dams to disposing materials. Constructing the core of a dam is an attractive use of geocontainers as a replacement of rock and rubble. For such an application, the water depth is usually within the range of 20 m (Bezuijen et al., 2002a; Oord, 1995), whereas disposing contaminated dredged materials is usually performed in deep water. Due to the water depth, which might reach 6000 m in the last application, a vortex shedding is expected to cause big change in the container shape. Different numerical models can be adopted according to the problem type; however, the deep dumping problem requires precise solving of the Navier-Stokes equation with a suitable turbulent model that is out of this research scope.

Performing large-scale measurement for dumping geocontainer is a demanding task requiring control of many parameters, depending on the objective of the experi-

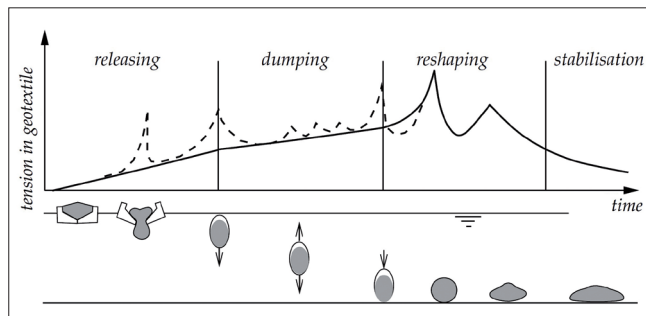


Figure 12: Geotextile forces during the dumping process after Pilarczyk (2000)

Bild 12: Während des Verklappens auf das Geotextil ausgeübte Kräfte nach Pilarczyk (2000)

ments. Installing geocontainer without tearing the geotextile is the most critical issue during the placement. When the container leaves the barge safely, it gains velocity during its travel through the water column. During this stage, no high tensile force is expected in the geotextile according to Figure 12, while the highest values are most probable during the impact of the container on the subsoil. In this section, the dumping phase of a field test is reproduced.

5.1 Field test of the sand-filled container *Feldversuch mit dem sandgefüllten Container*

The prototype test performed in 1994 by Oord (1995) is considered as a field measurement reference in this section. The test was carried out in the sand pit at Kekerdom in the Netherlands. Four geocontainers were dumped at different water depths. The aim of the test was to develop an appropriate method for dumping geocontainers without failure and to investigate their behaviour during dumping. As a conclusion of the test, two containers were failed during installation. The first failed very early due to quick release of the highly filled container, while the other failed later when it hit the ground due to the incorrect sand filling in the longitudinal direction. The unequal filling in the lateral direction causes rotation of the container, which in turn predicted higher vertical displacement than the real one. On the other hand, the measurements of the dumping velocity and the pressure inside the geocontainer are considered successful.

One of the two surviving geocontainers was filled with sand up to 130 m³, compared to the theoretical volume of 368 m³. It had a length of 24.5 m. Although the water

depth was 13 m, the fall height was approximated as 9.8 m assuming that the split barge was initially inside the water. Polypropylene woven geotextile GEOLON 120 was used having a specific mass of 630 g/m², and Young's modulus 1000 kN/m², with 120 kN/m tensile strength. Two longitudinal seams, having a strength of 70 % of the nominal value, were located on top of the container. Two places along the container length were selected to measure velocity and pressure. The front and rear sensors were placed about 3 m from the edges. The final inspection of the geocontainer after being placed was investigated by specific divers.

5.2 The MPM numerical model *Das numerische MPM-Modell*

Owing to limitations in the current implementation of the MPM model, the releasing phase is omitted from the simulation. The emphasis is on the dumping phase. To initialise the numerical model, the container is assumed to have an elliptical shape outside the barge. The dimensions of the ellipse oriented vertically are selected such that the length of the geotextile and the amount of the soil inside are the same as in the experiment. The soil container is placed inside water to resemble the height of the actual height in the experiment. The soil characteristics of the container and the subsoil layer are modelled using Mohr-Coulomb failure criteria as listed in Table 1. The viscosity of water is $\mu = 8.9 \cdot 10^{-4}$ Pa·s with the bulk modulus $K_f = 2.13$ GPa.

| property | unit | container | subsoil |
|--------------------|-------------------|-----------|-----------|
| unit weight | kN/m ³ | 16 | 20 |
| elasticity modulus | MPa | 2.8 | 10 |
| cohesion | kPa | 0 | 0 |
| Poisson's ratio | - | 0.333 | 0.333 |
| friction angle | degree | 30 | 30 |
| dilatancy angle | degree | 0 | 0 |
| drainage type | - | drained | undrained |

Table 1: Soils characteristics for dumping geocontainer in water

Tabelle 1: Bodenkennwerte für das Verklappen von Geocontainern im Wasser

The three dimensional problem is approximated as a plane-strain problem. A regular tetrahedral discretisation is adopted with finer mesh at the centre where the high deformation is expected. The configuration of the problem and the boundary conditions are shown in Figure 13. Similar to the lab test validation, initial hydrostatic pressure distribution is assumed for the water and K_0 condition for the soil considering the effect of the water column for the subsoil layer. The control point for checking vertical velocity and pressure is selected at the centre of the container.

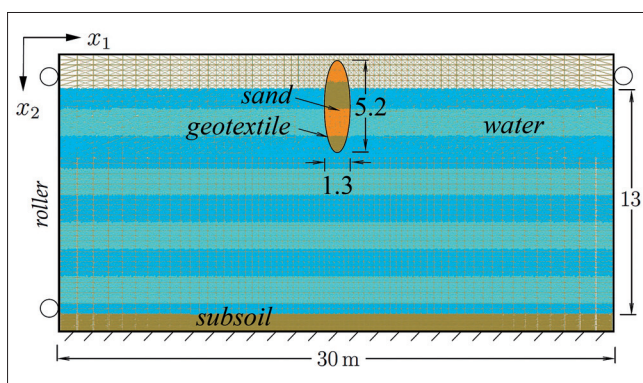


Figure 13: Initialisation of the MPM model for the sand-filled container

Bild 13: Initialisierung des MPM-Modells für den sandgefüllten Container

5.3 Comparison of the two models *Vergleich der beiden Modelle*

Owing to the uneven release of the prototype model in the experiment, an out-of-phase in the velocity of about 2 sec was recorded between the front and rear point as shown in Figure 14. Since the front part of the container was released first from the barge, it is pulled up due to the sticking of the rear end. In both curves, the first peak represents the releasing from the split barge stage while the second is when the container reaches the maximum velocity. The final inspection shows that the container rotated to the right ending up upside down. The vertical displacement of the container was determined by numerical integration of the given velocity, which gives an overestimation of the actual depth. The discrepancy between the calculated displacement and the real water depth was attributed to the geocontainer rotation where the measurement wires are pulled around the container leading to a larger measured depth (Oord, 1995).

Adel (1996) compared his analytical model with these measurements and predicted a value of 4.5 m/s for the terminal velocity without air. However, the last value reduces to the measured value 3.3 m/s when 17 % of air is assumed (Pilarczyk, 2000).

For the sake of comparison with the MPM container, the rear point is selected as a reference. Hence, the starting point of the MPM velocity is shifted to match the rear point of the prototype model. The trend of the numerical velocity matches the experimental in a quite reasonable manner for the accelerating part, while the MPM expects larger deceleration. In spite of eliminating air buoyancy in the MPM modelling, the terminal velocity is nicely estimated. The MPM velocity reaches the terminal velocity in about 3 sec. Shortly afterward it starts to feel the ground. The MPM displacement curve, see Figure 14, reflects the initial graduate accelerating and the steep decelerating at the end of the dumping phase. The smooth landing of the real container is likely due to the penetration of water through the permeable geotextile, which causes the container to drift to the side combined with flipping it upside down. No information is available regarding the final horizontal location.

The water pressure was measured inside the sand-filled container of the field experiment. As the MPM container is performed dry, the mean stress is calculated instead of the water pressure with a bar indicating the variation between the horizontal and vertical stress components as illustrated in Figure 14 with 0.96 as a coefficient of determination R^2 for the MPM curve. The lower peak of the front end was being related to the material escaping to the rear end, which was still falling (Oord, 1995). The MPM trend shows a little bump during the first 0.5 sec that is most likely because of the initial conditions; however, it catches quickly a straight behaviour that corresponds to the hydrostatic pressure. The difference between the vertical and horizontal stresses increases when the container approaches the bottom as the vertical component increases rapidly. The final residual value of the MPM mean stress reflects mainly the height of the water column 12 m while the experiment predicts about 8 m water column.

During dumping, the geocontainer shape changes drastically as demonstrated in Figure 15. Soil layering, which are initially horizontal as shown in Figure 13, helps the interpretation of the physical phenomena. At time 2 sec,

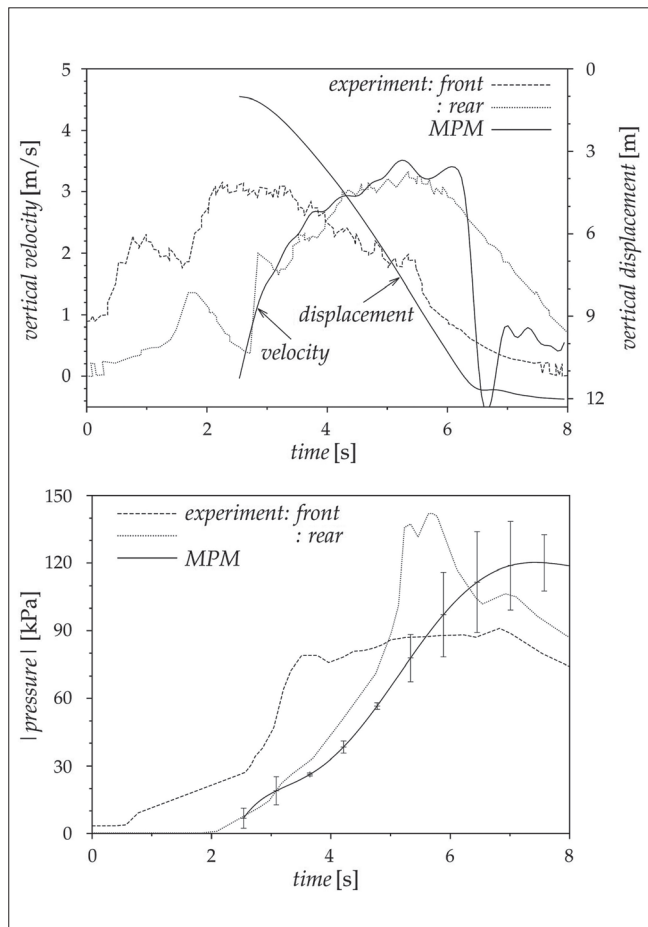


Figure 14: Comparison of the measured quantities (Oord, 1995) with the MPM results: (top) vertical velocity and (bottom) pressure

Bild 14: Vergleich der Messgrößen (Oord, 1995) und der Ergebnisse der MPM: (oben) vertikale Geschwindigkeit und (unten) Druck

the boundaries of the container are pulled up due to the drag being applied by the water flow while the bulb is moving downward. During the falling, not much tensile force is exerted on the geotextile and it is nearly homogeneous around the bag. A maximum value of 10 kN/m is recorded at the middle of the geotextile that indicates the symmetry of the external hydrodynamic forces. At time 4 sec, the geocontainer already touches the subsoil layer and starts to tilt to the right. The core part of the soil is pushed downward inducing 70 kN/m maximum tensile force in the lower left part of the container as shown in Figure 14. Checking the tensile force distribution, the upper half of the bag does not experience high forces. Owing to the clock-wise tilting, the geocontainer slides on the ground to the left direction producing tensile force along the membrane in contact with the seabed. Proceeding further with the simulation shows that the sand-filled container laid down to

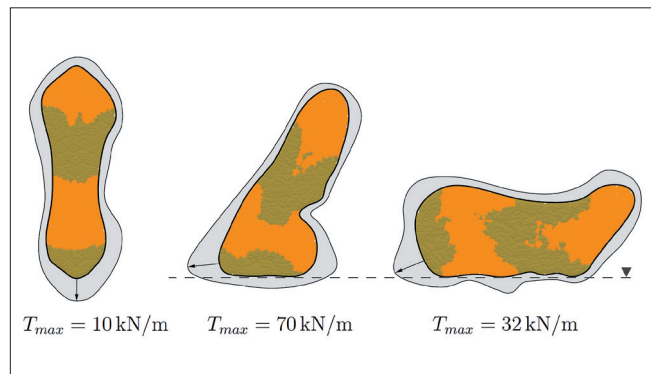


Figure 15: Reshape of the sand-filled container with the geotextile tensile force at 2 sec (left), 4 sec (middle), and 6 sec (right)

Bild 15: Änderung der Form des sandgefüllten Containers bei Beanspruchung des Geotextils durch Zugkräfte nach 2 s (links), 4 s (Mitte) und 6 s (rechts)

the side while it becomes more rectangular in shape. At the same time of 6 sec, the tensile forces become more homogeneous around the soil bag except for some irregularity along the subsoil layer.

It is important to indicate here that the assumption of rough geotextile-soil contact is expected to have a role on the final geocontainer configuration. For instance, a simulation using distinct element method showed that the soil is separated from the geotextile when the container reaches the ground (Palmerton, 1996). On the other hand, the current implementation forces the membrane to follow the soil with no gap. Therefore, the membrane might pull the soil in opposite direction to its movement, see the soil layering in the upper half at time 4 sec. Nonetheless, the aim of this study is to estimate the maximum tensile force during the dumping phase, which is shown to take place at the lower half where the material is compressed.

In the present analysis and for the requirement of the fluid modelling, the major part of the considered problem is the fluid material. Hence, the geocontainer itself is discretised relatively coarse. Combining this with the fact that MPM always smears the interface over one computational cell, a thick layer of non-uniform stresses is expected around the geocontainer. Refining the mesh as a quick remedy for this problem would become computationally expensive, especially if we remember that the fluid bulk modulus is the bottleneck of the time step size. Thinking about silent boundary for the water should reduce the problem size; however, care should be taken when fluid particles cross such a boundary.

6 Conclusions

Zusammenfassung

The ability of the material point method (MPM) to model large deformations in granular material combined with geosynthetic material and water is presented in this paper where two phases of dropping geocontainers are simulated; the first is to release a large container filled with granular material from a split barge and the second is to drop it in water. The simulation of dropping a geocontainer in place demonstrates that the MPM model is capable of predicting the shape and thickness of the container, which is consistent with the criteria proposed by Pilarczyk (2000). The numerical alternative for having folds along the geotextile lengths seems to provide releasing with smaller barge opening, which is similar to the experimental observations. Furthermore, the MPM model also predicts vertical stresses that are consistent with what one would expect. Furthermore, it has been shown that the formulation can handle the interaction of two containers.

Keeping in mind that the current numerical model simplifies the application to a uniform two-dimensional problem, whereas nonuniformity in the experimental model leads to release one end earlier than the other. Nevertheless, the terminal velocity of the container is well predicted. Maximum calculated geotextile force is about 70 kN/m during the entire process, which is within the design limits of maximum tensile strength of the geotextile material. Although no measurement to check these forces is available, field examination observed that the geocontainer lands on the sea bed safely, which matches with the numerical estimation.

7 Acknowledgment

Danksagung

Part of this research is carried out within the GEO-INSTALL project (Modelling Installation Effects in Geotechnical Engineering) and received funding from the European Community through the program (Marie Curie Industry-Academia Partnerships and Pathways) under grant agreement no. PIAP-GA-2009-230638. The authors would like to acknowledge Deltares/The Netherlands for providing access to their MPM source code, which was further extended and developed to achieve the results in this paper.

8 References

Literatur

- Adel, H. D. (1996): Forces due to impact and deformation of geotubes (in Dutch). Technical report, Delft Geotechnics, report CO-345040.
- Bezuijen, A., Schrijver, R., Breteler, M., Berendesen, E., Pilarczyk, K. (2002a): Field tests on geocontainers. In Proceedings of 7th International Conference on Geosynthetics, Nice, France.
- Bezuijen, A., Oung, O., Breteler, M., Berendesen, E., Pilarczyk, K. (2002b): Model tests on geocontainers, placing accuracy and geotechnical aspects. Proceedings of 7th International Conference on Geosynthetics, 1001-1006.
- Groot, de M., Bezuijen, A., Pilarczyk, K. (2000): Forces in geocontainer geotextile during dumping from barge. In Proceedings of 2nd EuroGeo2, 623-628.
- Groot, de M., Breteler, M., Berendsen, E. (2004). Feasibility of geocontainers at the sea shore. In Proceedings of 29th ICCE conference, World Scientific: 3904-3913.
- Hamad, F., Westrich, B., Vermeer, P. (2012): MPM formulation with accurate integration for a 3D membrane and an application of releasing geocontainer from barge, 5th European Geosynthetics Congress (EuroGeo5). Valencia (Spain), 1:78-87.
- Hamad, F., Vermeer, P., Moormann, C. (2013): Development of a coupled FEM-MPM approach to model a 3D membrane with an application of releasing geocontainer from barge, Installation Effects in Geotechnical Engineering, 176-183.
- Hamad, F., Stolle, D., Vermeer, P. (2014): Modelling of membranes in the material point method with applications, International Journal for Numerical and Analytical Methods in Geomechanics 39, 833-853.
- Jassim, I., Hamad, F., Vermeer, P. (2011): Dynamic material point method with applications in geomechanics. In 2nd International Symposium on Computational Geomechanics (COMGEO II), Cavtat-Dubrovnik, Croatia, 27-29.

Leshchinsky, D., Leshchinsky, O., Ling, H., Gilbert, P. (1996): Geosynthetic tubes for confining pressurized slurry: some design aspects, *Journal of Geotechnical Engineering*, 122(8): 682-690.

Lucy, L. (1977). A numerical approach to the testing of the fission hypothesis. *The Astronomical Journal*, 82(12): 1013-1024.

Oord, van A. (1995): Report test programme geocontainers. Technical report, Internal report of van Oord ACZ B. V. and Nicolon B. V. The Netherlands.

Palmerton, J. (1996): Overview of code ScowDropSim-a distinct element method formulation. Confidential documents at Deltares, The Netherlands.

Pilarczyk, K. (2000): *Geosynthetics and Geosystems in Hydraulic and Coastal Engineering*, Taylor & Francis.

Stolle, D., Maitland, K., Hamad, F. (2014): . Incompressible flow strategies for ice creep. *Finite Elements in Analysis and Design*, 89: 67-76.

Sulsky, D., Zhou, S., Schreyer, H. (1995): Application of a particle-in-cell method to solid mechanics. *Computer Physics Communications*, 87(1): 236-252.

Tencate Geosynthetics North America (2007): *Geosystems for Shoreline Protection*.

Wieckowski, Z., Youn, S. Yeon, J. (1999). A particle-in-cell solution to the silo discharging problem. *International Journal for Numerical Methods in Engineering*, 45(9): 1203-1225.

York, A., Sulsky, D., Schreyer, H. (1999): The material point method for simulation of thin membranes. *International Journal for Numerical Methods in Engineering*, 44(10): 1429-1456.